HHS Public Access

Author manuscript

Cancer Res. Author manuscript; available in PMC 2019 April 15.

Published in final edited form as:

Cancer Res. 2018 April 15; 78(8): 1923–1934. doi:10.1158/0008-5472.CAN-17-1624.

LPA Induces Metabolic Reprogramming in Ovarian Cancer via a Pseudohypoxic Response

Ji Hee Ha[1,2,*], **Rangasudhagar Radhakrishnan**[1,*], **Muralidharan Jayaraman**[1,2], **Mingda Yan**, **Jeremy D. Ward**[1,2], **Kar-Ming Fung**[1,3], **Katherine Moxley**[1,4], **Anil K. Sood**[5], **Ciro Isidoro**[6], **Priyabrata Mukherjee**[1,3], **Yong Sang Song**[7], and **Danny N. Dhanasekaran**[1,2,#]

[1]Stephenson Cancer Center, The University of Oklahoma Health Sciences Center, Oklahoma City, OK 73104, USA

[2]Department of Cell Biology, The University of Oklahoma Health Sciences Center, Oklahoma City, OK 73104, USA

[3]Department of Pathology, The University of Oklahoma Health Sciences Center, Oklahoma City, OK 73104, USA

[4]Department of Obstetrics and Gynecology, The University of Oklahoma Health Sciences Center, Oklahoma City, OK 73104, USA

[5]Department of Gynecologic Oncology & Reproductive Medicine, and the Center for RNA Interference and Non-Coding RNA, The University of Texas MD Anderson Cancer Center, Houston, TX 77030, USA

[6]Università del Piemonte Orientale, Novara, Italy

[7]Cancer Research Institute, Seoul National University, College of Medicine, Seoul 151-921, Korea

Abstract

Although hypoxia has been shown to reprogram cancer cells toward glycolytic shift, the identity of extrinsic stimuli that induce metabolic reprogramming independent of hypoxia, especially in ovarian cancer, is largely unknown. In this study, we use patient-derived ovarian cancer cells and high-grade serous ovarian cancer cell lines to demonstrate that lysophosphatidic acid (LPA), a lipid growth factor and GPCR ligand whose levels are substantially increased in ovarian cancer patients, triggers glycolytic shift in ovarian cancer cells. Inhibition of the G protein α-subunit Gαi2 disrupted LPA-stimulated aerobic glycolysis. LPA stimulated a pseudohypoxic response via Rac-mediated activation of NADPH oxidase (NOX) and generation of reactive oxygen species (ROS), resulting in activation of HIF1α. HIF1α in turn induced expression of glucose transporter-1 (GLUT1) and the glycolytic enzyme hexokinase-2 (HKII). Treatment of mice bearing ovarian cancer xenografts with an HKII inhibitor, 3-bromopyruvate attenuated tumor growth and conferred a concomitant survival advantage. These studies reveal a critical role for LPA in metabolic reprogramming of ovarian cancer cells and identify this node as a promising therapeutic target in ovarian cancer.

[#]Corresponding author. danny-dhanasekaran@ouhsc.edu.
[*]Equal contribution

The authors declare that there is no conflict of interest

Keywords

ovarian cancer; LPA; Hypoxia; HIF1; Hexokinase-2; G-proteins; targeted therapy

INTRODUCTION

Cancer cells reprogram glucose metabolism to aerobic glycolysis to meet the increased anabolic demands of cell growth and proliferation. Association between cancer cells and aerobic glycolysis has been well-recognized for many years now (1). However, the significance of this observation in relation to cancer progression and the adaptive mechanism(s) underlying this association is beginning to be understood only now (2–7). Metabolic reprogramming in cancer cells primarily involves a shift to aerobic glycolysis with or without an effect on mitochondrial oxidative phosphorylation (8). This is often accompanied by dysregulated lipogenic metabolism and adaptive mitochondrial reprogramming, both of which can contribute to aerobic glycolysis (3, 8–11). Studies focused on defining the mechanism underlying metabolic reprogramming in cancer cells have identified a critical role for oncogenes such as Ras and Myc and tumor suppressors such as p53 and pRB. In addition to the intrinsic genetic and epigenetic mechanisms regulated by the oncogenes and tumor suppressors, several extrinsic stimuli including those of growth factors and hypoxic stress have been shown to induce metabolic reprogramming in cancer cells (12–15). Of the different extrinsic factors, hypoxia-induced oxidative stress involving hypoxia-inducible factor 1 α-subunit (HIF1α) has been shown to play a major role in orchestrating the molecular events required to induce aerobic glycolysis in solid tumors (11, 16). However, the identity of extrinsic growth factors that can induce metabolic programming, is largely unknown. In this context, the observations that ovarian cancer cells synthesize and release lysophosphatidic acid (LPA) into the internal milieu and LPA is present in a large quantity in the ascites and serum of ovarian cancer patients are highly significant. Taken together with our findings that LPA stimulates epithelial to mesenchymal transition of ovarian cancer cells via HIF1α even in normoxic conditions (17), it can be posited that LPA induces aerobic glycolysis in ovarian cancer through a pseudohypoxic response involving HIF1α. In our current study, we investigated the role of LPA in the glycolytic shift in ovarian cancer using patient-derived ovarian cancer cells and high-grade serous ovarian cancer cell-lines in a metabolic flux analyzer. Our results indicate that LPA stimulates a pseudohypoxic response via a conduit involving Rac- NOX-ROS-HIF1α with the resultant induced expression of glucose transporter-1 and the glycolytic enzyme hexokinase-2 (HKII). Consistent with the tumor-promoting role of this pseudohypoxic nexus, we demonstrate that the inhibition of HKII with 3-Bromopyruvate (3-BP) can attenuate ovarian cancer xenograft tumor growth along with a concomitant survival advantage in an ovarian cancer xenograft mouse model.

Materials and Methods

Cell lines

Kuramochi, SNU119, OV90, TOV112D, OVCA429, OVCAR8, and SKOV3-ip cells have been previously described and cell passaging was never exceeded eighteen (18, 19). The cell

lines obtained from NCI, ATCC, and Seoul National University were authenticated at IDEXX Bioresearch (Columbia, MO) using nine human short tandem repeat profile (20). Cells were monitored for mycoplasma contamination using previously published PCR-based protocol (21). Patient derived cell line ASC022315, ASC022415, ASC031915 were isolated from the ascites samples of patients at the Stephenson Cancer Center, University of Oklahoma Health Science Center, Oklahoma City, OK, USA. The study was approved by the OUHSC Office of Human Research Participant Protection (HRPP) Institutional Review Board (IRB) and samples were collected with the informed consent from the patients. The ascites derived ovarian cancer cells were maintained in MCDB:DMEM (1:1) supplemented with 10% FBS and 50 μg/mL streptomycin. For serum-starvation, the above media without serum was supplemented with 0.1% BSA Fraction V, heat-shock, fatty acid ultra-free (Roche, Indianapolis, IN), 50 U/mL penicillin and 50 μg/mL streptomycin (Mediatech). Lysophosphatidic acid (1-oleoyl-2-hydroxy-sn-glycero-3-phosphate) was obtained from Avanti Polar Lipids (Alabaster, AL) and dissolved into 10 mM stock solutions in PBS with 0.1% BSA and stored at −80°C until use. siRNAs against HIF1α, Gαi2, Rac1, Rac2, Rac3, Nox1, Nox2, Nox3, Nox4, Nox5, HKII, and the control ON-TARGETplus Non-targeting siRNA #1 were purchased from Dharmacon (Lafayette, CO). shRNA targeting $G\alpha_{12}$, $G\alpha_{13}$, $G\alpha_{q}$, $G\alpha_{i2}$ and nonsense shRNA as well as immunoblot analyses and quantifications of immunoreactive bands have been previously described and used (22). N-acetyl-L-cysteine (NAC) and Bromopyruvic acid (3-Bromo-2-oxpropionic acid) was obtained from Sigma (St. Louis, MO). Apocynin, and Ki16425 inhibitor was procured from Tocris Bioscience (Bristol, UK). The Rac1 inhibitor NSC23766 was from EMD Millipore (Billerica, MA). The HIF1α inhibitor, PX-478 was obtained from MedKoo Biosciences (Morrisville, NC).

Seahorse XFe96 Extracellular Flux Analysis

The extracellular acidification rate (ECAR) was determined in XFe96 Extracellular Flux analyzer (Seahorse Bioscience, Billerica, MA) using the XF Glycolysis Stress Kit (Seahorse Bioscience, Billerica, MA) by following the manufacturer's instructions. Briefly, based on cell density titration experiment carried out in our lab, the ovarian cancer cell lines were seeded at a density of 30,000 cells/ well in a XF96 cell culture microplate. The cells were then either serum starved, stimulated with LPA or treated with inhibitor based on the experimental protocol till the desired time. Before the start of the assay the medium from these cells were removed and washed with freshly prepared non-buffered XF assay medium supplemented with 2 mM glutamine. About 175 μl of the same XF assay media was added to the cells and incubated in a CO_2-free incubator for a minimum of one hour. Glycolysis stress test was carried out by adding 25 μl of the stock of the following reagents, from the kit at recommended intervals, to reflect the indicated final concentration viz., glucose (Glu; 10 mM), oligomycin (Om; 1 μM) and 2-deoxyglucose (2-DG; 50 mM). XFe96 assays consisted of sequential mixing, pausing and measurement cycles, and assays were performed three times in triplicates. The data was analyzed and exported using the Seahorse Wave software (Seahorse, Billerica, MA) to the GraphPad Prism (La Jolla, CA) to obtain the graphs and bar charts and also carry out statistical analyses.

Xenograft model

Nu/Nu nude female mice (5–6 weeks old) were purchased from Taconic Labs Inc. (Hudson, NY) and were housed in a barrier facility under 12hour light/ dark cycle under pathogen free conditions, with food and water ad libitum. All experiments were performed with the approval of the University of Oklahoma Health Science Center Institutional Animal Care and Use Committee. SKOV3-ip, and OVCAR8 cells at log phase (5×10^6 cells/100 μl) were injected on the right flank of nude female mice subcutaneously to generate tumors. When the tumors reached ~50 mm^3, the mice were randomized into control and treatment groups (SKOV3-ip; n=10, OVCAR8; n=5). The 3-BP (10 mg/kg/day) was diluted in sterile normal saline and injected intraperitoneally into the mice. The injections were carried out every day for 3 days on the first week and third week. Tumor volume was measured twice a week and recorded. At the study termination, tumor volumes were measured, animals were sacrificed, necropsy carried out to collect tumor specimens for immunohistochemical (IHC) staining.

IHC analysis

Tumors dissected out were fixed with 10% neutral formalin, paraffin-embedded, cut into 4 μm sections, mounted on positively charged slides and processed for immunohistochemical staining. The immunohistochemistry was performed according to manufacturer's protocol using Leica BondTM Polymer Refine Detection system (DS 9800). The slides were incubated at 60°C for 45 minutes followed by deparaffinization and rehydration in an automated Multistainer (Leica ST5020). Subsequently, these slides were transferred to the Leica Bond-IIITM, treated for target retrieval at 100°C for 20 minutes with a retrieval buffer, pH 6.0. Endogenous peroxidase was blocked using peroxidase-blocking reagent, followed by the primary antibody, rabbit monoclonal anti phosphohistone H3 (PHH3, 1:300, Sigma #369A) incubation. For the secondary antibody, post-primary IgG-linker and/or Poly-AP IgG reagents were used. The substrate chromogen, 3, 3′-diaminobenzidine tetrahydrochloride (DAB) detects the complex as brown precipitate, while hematoxylin counterstain the cell nuclei (blue). The slides were then dehydrated (Leica ST5020), and mounted (Leica MM24). Antibody specific positive and negative (omission of primary antibody) controls were parallel stained. HIF1α antibodies were purchased from BD Biosciences (San Jose, CA) whereas antibodies to GLUT1, HKII, GAPDH, Rac1, HKII and β-actin were obtained from Cell Signaling Technologies (Danvers, MA), Rac3, Nox1, Nox2, Nox3, Nox4 and Nox5 were obtained from Abcam (Cambridge, MA), Rac2 is from ThermoFisher (Carlsbad, CA), and Gα12, Gα13, Gαq, and Gαi2 antibodies were purchased from Santa Cruz Biotechnology (Santa Cruz, CA).

Patient Samples

Ascites from which the patient-derived cells used in this study were obtained through Stephenson Cancer Center Biospecimen core with written informed consent from patients and the studies were conducted in accordance with the ethical principles and guidelines set forth in the "Belmont Report", the Declaration of Helsinki, and the Nuremberg Code. In addition, the University of Oklahoma adheres to the Office for Human Research Protection (OHRP) requirements, as set forth in 45 CFR 46 and its subparts A, B, C, and D, and the FDA in 21 CFR 50 and 56.

Scoring of mitotic figures

Mitotic figures on PHH3 IHC slides were counted using ImageJ NIH software on 5 fields for each slide in triplicates at 20× magnification. Only cells with metaphase or anaphase morphology were considered positive. The numerated PHH3 mitotic figures from control and treated xenograft tumor sections were tabulated and statistically analyzed for significance using t-test.

Statistical analysis

All statistical analysis was performed using GraphPad Prism (La Jolla, CA) by two-tailed student's *t*-test with Welch's correction.

RESULTS

LPA stimulates aerobic glycolysis in ovarian cancer cells

To determine the role of LPA in inducing glycolytic shift in ovarian cancer cells, we monitored glycolysis and glycolysis capacity by monitoring the extracellular acidification rate (ECAR) in ovarian cancer cell lines. To rule out the role for any signature oncogene or tumor suppressor gene in this regulation, our test panel consisted of ovarian cancer cell lines representing different genetic background as well as diverse ovarian cancer subtypes. A series of time course experiments with different doses of LPA were carried out to monitor ECAR in response to the addition of glucose, oligomycin, and 2-deoxyglucose. Glucose was added to initiate glycolysis and the ECAR flux observed following the addition of glucose was used to determine glycolytic rate. ECAR following the addition of oligomycin represented the overall glycolytic capacity of the cells whereas the difference in ECAR before and after the addition of oligomycin defined the glycolytic reserve of the cells. As shown in Figure 1, LPA induced an increase in both the rate of glycolysis and glycolytic capacity in all tested ovarian cancer cells irrespective of their genetic background or subtype categories. LPA is present in large concentration in the ascitic fluid that constantly baths the ovarian cancer. Thus, it can be postulated that the LPA present in the ascites stimulate such a pathological shift towards aerobic glycolysis in ovarian cancer cells. To test this possibility, we stimulated ovarian cancer cells derived from HGSOC patients with varying concentrations of LPA and determined the ECAR. As shown in Figure 2, LPA stimulated an increase in aerobic glycolysis as well as the glycolytic capacity of these patient-derived ovarian cancer cells, thus establishing a causative role for LPA in metabolic reprogramming of ovarian cancer cells.

LPA-stimulated metabolic reprogramming involves Gαi2

LPA is known to stimulate its biological responses through G protein-coupled LPA receptors (LPARs). Consistent with this view, treating the cells with LPA-antagonists blocked LPA-stimulated ECAR in SKOV3 cells (Figure S1). Our previous studies have shown that LPA transmits diverse oncogenic signals through specific G protein α-subunits, namely Gαi, Gαq, Gα12, and Gα13. To identify the Gα-subunit involved in transmitting the metabolic reprogramming stimuli from LPA, we carried out ECAR flux analyses using SKOV3 cells in which the individual Gα-subunit was silenced using siRNA. Our results indicated that LPA-

stimulated glycolytic shift primarily involves Gαi2 since the silencing of Gαi2 with specific siRNA led to the attenuation of both the rate of glycolysis and glycolytic capacity as indicated by the ECAR flux in OVCA429 (Figure 3A) as well as in SKOV3-ip cells (Figure 3B), while the silencing of other Gα-subunits failed to have such an effect (Figure S2).

Regulation of glycolysis by LPA requires Rac1-NOX-ROS- network

Previously, we have shown that LPA activates EMT in ovarian cancer cells via Gαi2-stimulated HIF1α (17). In addition, previous studies have shown that Gαi2 can lead to the activation of Rac (23) and Rac, once activated, can stimulate the ROS-generating NOX-family of NADPH oxidases, resulting in an increase in the intracellular levels of ROS (24). Furthermore, ROS-mediated inhibition of prolyl hydroxylase doamain-2 enzyme, which is involved in ubiquitin-mediated degradation of HIF1α, can lead to an increase in the levels of HIF1α levels (25–28), which plays a critical role in cellular hypoxic response and hypoxia-mediated metabolic reprogramming in cancer cells. Based on these studies, we reasoned that the LPA-LPAR-Gαi2 axis could induce a pseudohypoxic response involving the Rac-NOX-ROS-HIF1α pathway that ultimately leads to the metabolic reprogramming in ovarian cancer cells. To validate this rationale, we first tested whether Rac1 is required for LPA-mediated ECAR flux. Our results indicated that the inhibition of Rac1 with Rac1-specific inhibitor attenuated LPA-stimulated glycolytic shift in ovarian cancer cells represented by SNU119 (Figure 4A) SKOV3 cells (Figure S3). Consistent with these findings, siRNA-mediated silencing the expression of Rac1 in OVCA429 cells inhibited LPA-mediated glycolysis (Figure 4B). In contrast, silencing of Rac2 or Rac3 failed to have such effect (Figure S4). Next, we investigated the role of downstream NADPH oxidase in this signaling network. SNU119 and SKOV3 cells were treated with apocynin, an inhibitor of NADPH oxidase and LPA-stimulated ECAR was monitored. Results indicated that inhibiting NOX led to the blunting of LPA-stimulated increase in glycolysis as well as glycolytic capacity in both the cell lines (Figure 4C and Figure S3). Using siRNA specific to NOX2, it can be shown that the silencing of NOX2 in OVCA429 cells (Figure 4D) attenuated LPA-stimulated aerobic glycolysis while silencing of NOX1, NOX3, NOX4, or NOX5 failed to do so (Figure S5). Similarly, treating the cells with ROS-scavenger N-acetyl-L-cysteine abrogated LPA-stimulated glycolysis (Figure 4E and Figure S3).

LPA elicits a pseudohypoxic response with an increase in HIF1α to promote aerobic glycolysis

With our previous findings that LPA stimulates an increase in HIF1α levels and activity via Gαi2 (17) along with the observations from several laboratories that ROS could stabilize and increase the levels of HIF1α levels (25–28), it can be reasoned that the LPA induces metabolic programming in ovarian cancer cells by eliciting a pseudohypoxic response that leads to an increase in HIF1α levels via Rac-NOX-ROS signaling conduit. It can also be surmised that HIF1α, thus stabilized, promotes metabolic reprogramming in ovarian cancer cells. To validate this paradigm, first we investigated whether the inhibition of Rac, NOX, or scavenging ROS could abrogate the increase in HIF1α levels. As shown in Figure 5A, the inhibition of Rac or NOX or ROS abrogated LPA-stimulated increase in the levels of HIF1α in SNU119 cells (Figure 5A). Next, we investigated whether the inhibition of HIF1α abrogated LPA-stimulated aerobic glycolysis in ovarian cancer cells. This was carried out

using PX-478, an inhibitor that reduces the expression of HIF1α through multiple mechanisms (17, 29). Kuromochi or SNU119 cells were pretreated with PX-478 and LPA-stimulated glycolysis was monitored. As shown in Figure 5, the inhibition of HIF1α by PX-478 (Fig. 5B & C) significantly reduced aerobic glycolysis in both Kuromochi and SNU119 cells. Thus, our findings establish that LPA stimulates aerobic glycolysis by eliciting a pseudohypoxic response leading to an increase in HIF1α levels, which in turn, promotes aerobic glycolysis in ovarian cancer cells.

LPA stimulated glycolysis involves of GLUT1 and HKII through Gαi2 and HIF1α

Generally, HIF1α expression and activation occur in hypoxic region of tumor cells and it has been shown that HIF1α plays a determinant role in promoting glycolytic shift in hypoxic tumor cells (30–32). During hypoxia, HIF1α has been shown to induce glycolytic shift in tumor cells by transactivating the expression of genes involved in glucose/glycolysis metabolism and mitochondrial functions (30). It can be observed that LPA stimulated an increase in levels of HIF1α by 2.5 minutes (Figure S6) along with the stimulation of its transcriptional activity by 20 minutes (17). Of the genes that are transcriptionally upregulated by HIF1α, increased expression of glucose transporter-1 (GLUT1) and hexokinase-2 (HKII) have been correlated with glycolytic shift in multiple cancers cells and tissues (8, 33–35). Therefore, we examined whether the observed LPA-Gαi2-HIF1α mediated aerobic glycolysis involves the expression GLUT1 and HKII. SKOV3-ip cells in which the expression of Gαi2 or HIF1α was knocked down using specific siRNAs were stimulated with LPA and the expression levels of GLUT1 and HKII were monitored. As shown in Fig. 6, LPA stimulated the expression of both GLUT1 and HKII whereas the silencing the expression of Gαi2 blunted LPA-stimulated expression of HIF1α, GLUT1, and HKII (Figure 6A). Likewise, silencing the expression of HIF1α led to a decrease in LPA-stimulated expression of GLUT1 and HKII (Fig. 6B). Next, we investigated whether the increased HKII levels contribute to LPA-stimulated aerobic glycolysis. This was assessed using siRNA to HKII in OVCA429 cells. As shown in Figure 6C, silencing of HKII drastically attenuated LPA-stimulated glycolysis in these cells.

Therapeutic Potential of Targeting HKII in Ovarian Cancer

In addition to establishing the Gαi2-Rac-NOX-ROS-HIF1α signaling axis in LPA-stimulated glycolytic response, these results also point to the metabolic nodes stimulated by LPA as potential therapeutic targets in ovarian cancer. This is further supported by the observations that the glycolytic pathway inhibitors could attenuate the proliferation of diverse cancer cells including ovarian cancer cell lines (36). Although the components of glycolytic pathway such as GLUT1, HKII, pyruvate kinases-M2, and lactate dehydrogenase-A have been evaluated for their efficacy as chemotherapeutic targets in many cancers (37, 38), there is a paucity of such information in the context of ovarian cancer. It is significant to note here that HKII is overexpressed in ovarian cancer tissues (39) and it has been identified as a negative prognostic factor in many cancers (40–42). Therefore, we interrogated whether HKII could serve as a therapeutic target in ovarian cancer. To test, we used two independent ovarian cancer cell-line derived xenograft (CDX) mouse models in vivo using SKOV3-ip and OVCAR8 cell lines. SKOV3-ip or OVCAR8 cells were injected subcutaneously into the right flank and the animals were examined every day for the appearance of palpable tumors.

When the tumors reached 50 mm^3 (day-11), 3-bromopyruvate (3-BP) was intraperitoneally administered in two cycles. Tumor growth in these animals were monitored and the studies were terminated at day 36, before the animal welfare was compromised. As shown in Figure 7, the administration of 3-BP inhibited the growth of both SKOV3-ip and OVCAR8 xenograft tumors. A reduction in tumor volume was observed from day-14 following the administration of 3-BP in SKOV3-ip xenograft tumors (Figure 7A & B) along with a significant regression in tumor growth (Figure 7C). Tumors harvested from these animals were processed for immunohistochemical analysis using anti-phosphohistone H3 antibodies (anti-PHH3) to determine the mitotic index of the cells. Results indicated that the mitotic figures labeled by anti-PPH3 were greatly reduced in cancer tissues derived from 3-BP treated animals (Figure 7D). Quantification of the data indicated that the residual tumor tissue derived from 3-BP treated animals showed 75% reduction in mitotic cells, indicating the inhibitory effect of 3-BP on mitotic proliferation (Figure 7E). A reduction in tumor volume could also be seen in OVCAR8 xenograft tumors from day-3 onwards following 3-BP treatment (Figure 7F & G). Anti-PPH3-staining of OVCAR8 xenograft tumor tissues from 3-BP treated animals showed a similar decrease in mitotic index (Figure 7H & I). Together, these findings identify the signaling nodes in aerobic glycolysis modulated by LPA - especially that of HKII - as potential therapeutic targets in ovarian cancer.

DISCUSSION

Despite newer findings on the etiology and biology of ovarian cancer, it still remains the most lethal gynecologic cancer with the five-year survival rate of 47% (43). While there has been a marginal increase in five-year survival over the past 10-years, an effective targeted therapy for ovarian cancer is still lacking. Despite the observation that ovarian cancer patients respond very well to the initial platinum-based therapy, they often suffer from disease recurrence. The absence of an effective targeted therapy is one of the factors that has contributed to the relatively marginal improvement in patient survival seen with ovarian cancer. Newer regimens targeting angiogenesis and polyadenosine diphosphate (ADP)-ribose polymerases are being adapted as second-line therapies for relapsing ovarian cancer, their effect on overall survival is rather modest (44). In addition, the etiological and genetic dichotomy underlying type I and type II ovarian cancers as well as the subtypes within each of them pose significant challenges in the development of an effective targeted therapy regimen. Based on the observations that almost all of the recurrent ovarian cancer patients present with ascites (45, 46) and the ascitic fluid contain a high concentration of LPA, which promotes both mitogenic and motogenic signaling (47, 48), several laboratories including ours have focused on identifying a therapeutic target in LPA-signaling nodes. As previously discussed (17), targeting LPA-receptors has proven to be a non-viable strategy due the high concentration of LPA in the ascites as well as the presence of LPA-synthetic machinery in close proximity to LPARs in the membrane. Thus, it is of critical interest to identify the signaling nodes downstream of LPARs that can serve as potential therapeutic target in ovarian cancer. With this overarching goal, our previous studies have shown that LPA could stimulate the epithelial to mesenchymal transition in ovarian cancer cells through Gαi2-dependent increase in the levels of HIF1α (17). Our current study extends these findings further by demonstrating the role of LPA in orchestrating a pseudohypoxic response that

induces metabolic reprogramming in ovarian cancer cells towards aerobic glycolysis. Our results also indicate that this particular LPA-stimulated signaling node involving Gαi2, Rac, NOX, ROS, and HIF1α is independent of ovarian cancer subtypes and the mutational status of the genes associated with these subtypes including p53 and BRCA1/2. More significantly, we demonstrate here the therapeutic potential of targeting HKII, a downstream link in LPA-stimulated metabolic programming, in inhibiting ovarian cancer growth using a preclinical CDX-mouse model.

Previous studies from several laboratories including ours have shown that LPA stimulates an increase in HIF1α levels in ovarian cancer cells. While the role of HIF1α in metabolic programming in tumor cell hypoxia is well known, its role in LPA-mediated metabolic reprogramming in normoxia is largely uncharacterized. Likewise, the mechanism by which LPA rapidly upregulates the levels and activity of HIF1α has not been elucidated. Our observation that LPA stimulated increase in HIF1α levels and activity could be seen by 2.5 minutes is the first report of its kind and it indicates that the effect of LPA on metabolic reprogramming via this signaling nexus is an acute and rapid event. Furthermore, our findings that LPA stimulates an increase in HIF1α levels via Rac-NOX-ROS conduit and that this signaling nexus is critically involved in LPA-mediated metabolic reprogramming are quite novel and hitherto unreported. In addition, with the use of multiple ovarian cancer cell lines with varying genetic mutational signatures (Fig. 1), we demonstrate here that the metabolic reprogramming regulated by LPA is not dependent on p53, MYC, or BRCA1/2, PI3K, PTEN, or KRAS mutations. Such a similitude of response elicited by LPA in all of the cell lines, identifies this signaling nexus as a potential candidate for targeted therapy in ovarian cancer. Finally, the importance of this pathway is further validated by our results using CDX-animal studies. Our observation that HKII inhibitor significantly attenuated the growth of the ovarian cancer xenograft tumor growth, highlights the overall importance of this pathway in ovarian cancer progression and its potential for specific targeting in ovarian cancer patients.

Supplementary Material

Refer to Web version on PubMed Central for supplementary material.

Acknowledgments

This research was supported by National Institutes of Health grants CA116984, CA123233 (to D.N. Dhanasekaran), GM103639 (to D.N. Dhanasekaran & J.H. Ha) and Priority Research Centers Program grant 2009-0093820, the BK21 Plus Program grant 5256-20140100 (Y.S. Song) through the National Research Foundation of Korea (to Y.S. Song). We also thank the Stephenson Cancer Center, OUHSC, Oklahoma City, OK; Mary K. Chapman Foundation Grant Award for Stephenson Cancer Center-MD Anderson Collaborative Research initiative (D.N. Dhanasekaran, K. Moxley, and A.K. Sood) and an Institutional Development Award (IDeA) from the National Institute of General Medical Sciences of the National Institutes of Health under grant P20 GM103639 for the tissue pathology, IHC analysis, and fluorescence imaging services.

References

1. Warburg O, Wind F, Negelein E. The Metabolism of Tumors in the Body. J Gen Physiol. 1927; 8(6): 519–30. [PubMed: 19872213]
2. Ferreira LM, Hebrant A, Dumont JE. Metabolic reprogramming of the tumor. Oncogene. 2012; 31(36):3999–4011. [PubMed: 22231450]

3. Sciacovelli M, Gaude E, Hilvo M, Frezza C. The metabolic alterations of cancer cells. Methods Enzymol. 2014; 542:1–23. [PubMed: 24862258]
4. Iurlaro R, Leon-Annicchiarico CL, Munoz-Pinedo C. Regulation of cancer metabolism by oncogenes and tumor suppressors. Methods Enzymol. 2014; 542:59–80. [PubMed: 24862260]
5. Potter M, Newport E, Morten KJ. The Warburg effect: 80 years on. Biochem Soc Trans. 2016; 44(5):1499–505. [PubMed: 27911732]
6. Pavlova NN, Thompson CB. The Emerging Hallmarks of Cancer Metabolism. Cell Metab. 2016; 23(1):27–47. [PubMed: 26771115]
7. Vander Heiden MG, DeBerardinis RJ. Understanding the Intersections between Metabolism and Cancer Biology. Cell. 2017; 168(4):657–69. [PubMed: 28187287]
8. Hay N. Reprogramming glucose metabolism in cancer: can it be exploited for cancer therapy? Nat Rev Cancer. 2016; 16(10):635–49. [PubMed: 27634447]
9. Beloribi-Djefaflia S, Vasseur S, Guillaumond F. Lipid metabolic reprogramming in cancer cells. Oncogenesis. 2016; 5:e189. [PubMed: 26807644]
10. Zong WX, Rabinowitz JD, White E. Mitochondria and Cancer. Mol Cell. 2016; 61(5):667–76. [PubMed: 26942671]
11. DeBerardinis RJ, Chandel NS. Fundamentals of cancer metabolism. Sci Adv. 2016; 2(5):e1600200. [PubMed: 27386546]
12. Nakazawa MS, Keith B, Simon MC. Oxygen availability and metabolic adaptations. Nat Rev Cancer. 2016; 16(10):663–73. [PubMed: 27658636]
13. Saxton RA, Sabatini DM. mTOR Signaling in Growth, Metabolism, and Disease. Cell. 2017; 168(6):960–76. [PubMed: 28283069]
14. Lee SY, Jeong EK, Ju MK, Jeon HM, Kim MY, Kim CH, et al. Induction of metastasis, cancer stem cell phenotype, and oncogenic metabolism in cancer cells by ionizing radiation. Mol Cancer. 2017; 16(1):10. [PubMed: 28137309]
15. Nagarajan A, Malvi P, Wajapeyee N. Oncogene-directed alterations in cancer cell metabolism. Trends Cancer. 2016; 2(7):365–77. [PubMed: 27822561]
16. Panieri E, Santoro MM. ROS homeostasis and metabolism: a dangerous liason in cancer cells. Cell Death Dis. 2016; 7(6):e2253. [PubMed: 27277675]
17. Ha JH, Ward JD, Radhakrishnan R, Jayaraman M, Song YS, Dhanasekaran DN. Lysophosphatidic acid stimulates epithelial to mesenchymal transition marker Slug/Snail2 in ovarian cancer cells via Galphai2, Src, and HIF1alpha signaling nexus. Oncotarget. 2016
18. Ha JH, Yan M, Gomathinayagam R, Jayaraman M, Husain S, Liu J, et al. Aberrant expression of JNK-associated leucine-zipper protein JLP, promotes accelerated growth of ovarian cancer. Oncotarget. 2016; 7(45):72845–59. [PubMed: 27655714]
19. Gomathinayagam R, Muralidharan J, Ha JH, Varadarajalu L, Dhanasekaran DN. Hax-1 is required for Rac1-Cortactin interaction and ovarian carcinoma cell migration. Genes Cancer. 2014; 5(3–4): 84–99. [PubMed: 25053987]
20. Ruitberg CM, Reeder DJ, Butler JM. STRBase: a short tandem repeat DNA database for the human identity testing community. Nucleic Acids Res. 2001; 29(1):320–2. [PubMed: 11125125]
21. Choppa PC, Vojdani A, Tagle C, Andrin R, Magtoto L. Multiplex PCR for the detection of Mycoplasma fermentans, M. hominis and M. penetrans in cell cultures and blood samples of patients with chronic fatigue syndrome. Mol Cell Probes. 1998; 12(5):301–8. [PubMed: 9778455]
22. Ha JH, Gomathinayagam R, Yan M, Jayaraman M, Ramesh R, Dhanasekaran DN. Determinant role for the gep oncogenes, Galpha12/13, in ovarian cancer cell proliferation and xenograft tumor growth. Genes Cancer. 2015; 6(7–8):356–64. [PubMed: 26413218]
23. Ward JD, Ha JH, Jayaraman M, Dhanasekaran DN. LPA-mediated migration of ovarian cancer cells involves translocalization of Galphai2 to invadopodia and association with Src and beta-pix. Cancer Lett. 2015; 356(2 Pt B):382–91. [PubMed: 25451317]
24. Bedard K, Krause KH. The NOX family of ROS-generating NADPH oxidases: physiology and pathophysiology. Physiol Rev. 2007; 87(1):245–313. [PubMed: 17237347]

25. Gerald D, Berra E, Frapart YM, Chan DA, Giaccia AJ, Mansuy D, et al. JunD reduces tumor angiogenesis by protecting cells from oxidative stress. Cell. 2004; 118(6):781–94. [PubMed: 15369676]
26. Hagen T. Oxygen versus Reactive Oxygen in the Regulation of HIF-1alpha: The Balance Tips. Biochem Res Int. 2012; 2012:436981. [PubMed: 23091723]
27. Li YN, Xi MM, Guo Y, Hai CX, Yang WL, Qin XJ. NADPH oxidase-mitochondria axis-derived ROS mediate arsenite-induced HIF-1alpha stabilization by inhibiting prolyl hydroxylases activity. Toxicol Lett. 2014; 224(2):165–74. [PubMed: 24188932]
28. Lee G, Won HS, Lee YM, Choi JW, Oh TI, Jang JH, et al. Oxidative Dimerization of PHD2 is Responsible for its Inactivation and Contributes to Metabolic Reprogramming via HIF-1alpha Activation. Sci Rep. 2016; 6:18928. [PubMed: 26740011]
29. Koh MY, Spivak-Kroizman T, Venturini S, Welsh S, Williams RR, Kirkpatrick DL, et al. Molecular mechanisms for the activity of PX-478, an antitumor inhibitor of the hypoxia-inducible factor-1alpha. Mol Cancer Ther. 2008; 7(1):90–100. [PubMed: 18202012]
30. Denko NC. Hypoxia, HIF1 and glucose metabolism in the solid tumour. Nat Rev Cancer. 2008; 8(9):705–13. [PubMed: 19143055]
31. Mujcic H, Hill RP, Koritzinsky M, Wouters BG. Hypoxia signaling and the metastatic phenotype. Curr Mol Med. 2014; 14(5):565–79. [PubMed: 24894165]
32. Semenza GL. HIF-1 mediates metabolic responses to intratumoral hypoxia and oncogenic mutations. J Clin Invest. 2013; 123(9):3664–71. [PubMed: 23999440]
33. Wolf A, Agnihotri S, Micallef J, Mukherjee J, Sabha N, Cairns R, et al. Hexokinase 2 is a key mediator of aerobic glycolysis and promotes tumor growth in human glioblastoma multiforme. J Exp Med. 2011; 208(2):313–26. [PubMed: 21242296]
34. Porporato PE, Dhup S, Dadhich RK, Copetti T, Sonveaux P. Anticancer targets in the glycolytic metabolism of tumors: a comprehensive review. Front Pharmacol. 2011; 2:49. [PubMed: 21904528]
35. Wang J, Ye C, Chen C, Xiong H, Xie B, Zhou J, et al. Glucose transporter GLUT1 expression and clinical outcome in solid tumors: a systematic review and meta-analysis. Oncotarget. 2017
36. Zhao Y, Butler EB, Tan M. Targeting cellular metabolism to improve cancer therapeutics. Cell Death Dis. 2013; 4:e532. [PubMed: 23470539]
37. Hamanaka RB, Chandel NS. Targeting glucose metabolism for cancer therapy. J Exp Med. 2012; 209(2):211–5. [PubMed: 22330683]
38. Vander Heiden MG. Targeting cancer metabolism: a therapeutic window opens. Nat Rev Drug Discov. 2011; 10(9):671–84. [PubMed: 21878982]
39. Jin Z, Gu J, Xin X, Li Y, Wang H. Expression of hexokinase 2 in epithelial ovarian tumors and its clinical significance in serous ovarian cancer. Eur J Gynaecol Oncol. 2014; 35(5):519–24. [PubMed: 25423696]
40. Palmieri D, Fitzgerald D, Shreeve SM, Hua E, Bronder JL, Weil RJ, et al. Analyses of resected human brain metastases of breast cancer reveal the association between up-regulation of hexokinase 2 and poor prognosis. Mol Cancer Res. 2009; 7(9):1438–45. [PubMed: 19723875]
41. Huang X, Liu M, Sun H, Wang F, Xie X, Chen X, et al. HK2 is a radiation resistant and independent negative prognostic factor for patients with locally advanced cervical squamous cell carcinoma. Int J Clin Exp Pathol. 2015; 8(4):4054–63. [PubMed: 26097593]
42. Ogawa H, Nagano H, Konno M, Eguchi H, Koseki J, Kawamoto K, et al. The combination of the expression of hexokinase 2 and pyruvate kinase M2 is a prognostic marker in patients with pancreatic cancer. Mol Clin Oncol. 2015; 3(3):563–71. [PubMed: 26137268]
43. Siegel RL, Miller KD, Jemal A. Cancer Statistics, 2017. CA Cancer J Clin. 2017; 67(1):7–30. [PubMed: 28055103]
44. Coward JI, Middleton K, Murphy F. New perspectives on targeted therapy in ovarian cancer. Int J Womens Health. 2015; 7:189–203. [PubMed: 25678824]
45. Ahmed N, Stenvers KL. Getting to know ovarian cancer ascites: opportunities for targeted therapy-based translational research. Front Oncol. 2013; 3:256. [PubMed: 24093089]
46. Smolle E, Taucher V, Haybaeck J. Malignant ascites in ovarian cancer and the role of targeted therapeutics. Anticancer Res. 2014; 34(4):1553–61. [PubMed: 24692682]

47. Fang X, Schummer M, Mao M, Yu S, Tabassam FH, Swaby R, et al. Lysophosphatidic acid is a bioactive mediator in ovarian cancer. Biochim Biophys Acta. 2002; 1582(1–3):257–64. [PubMed: 12069836]

48. Pua TL, Wang FQ, Fishman DA. Roles of LPA in ovarian cancer development and progression. Future Oncol. 2009; 5(10):1659–73. [PubMed: 20001802]

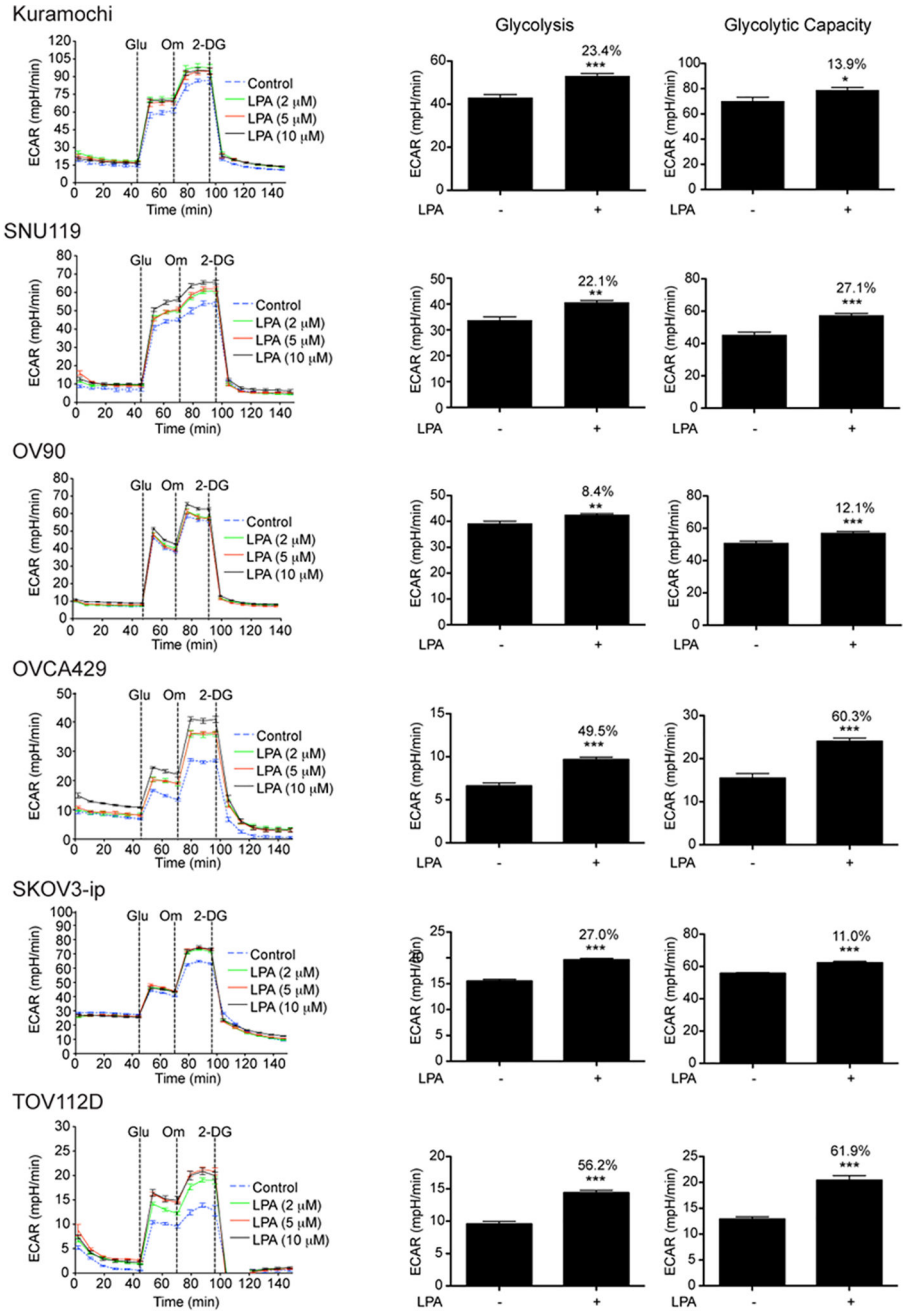

Figure 1. LPA stimulates aerobic glycolysis in ovarian cancer cells

Serum-starved ovarian cancer cell lines, Kuramochi, SNU119, OV90, OVCA-429, SKOV3-ip, and TOV112D were stimulated 2, 5, and 10 μM concentration of LPA for 6 h and ECAR was determined using XFe96 extracellular flux analyzer. ECAR was measured every 8 minutes (Left Panel). Addition of glucose (10 mM), oligomycin (1 μM) and 2-DG (50 mM) were carried out at the indicated time-points. Rate of glycolysis and glycolytic capacity derived from the ECAR analysis with LPA-stimulation (10 μM) are presented as bar charts. Every experiment was repeated at least three times and the results are from a representative analysis. Error bars indicate mean ± SEM (n = 5 to 21parallel determinations). Percentile

increases over the basal levels of glycolysis and glycolytic capacity are denoted above the bars of the chart. Statistical significance between LPA-treated and untreated cells was determined by Student's t test (**P<0.005; ***P<0.0005).

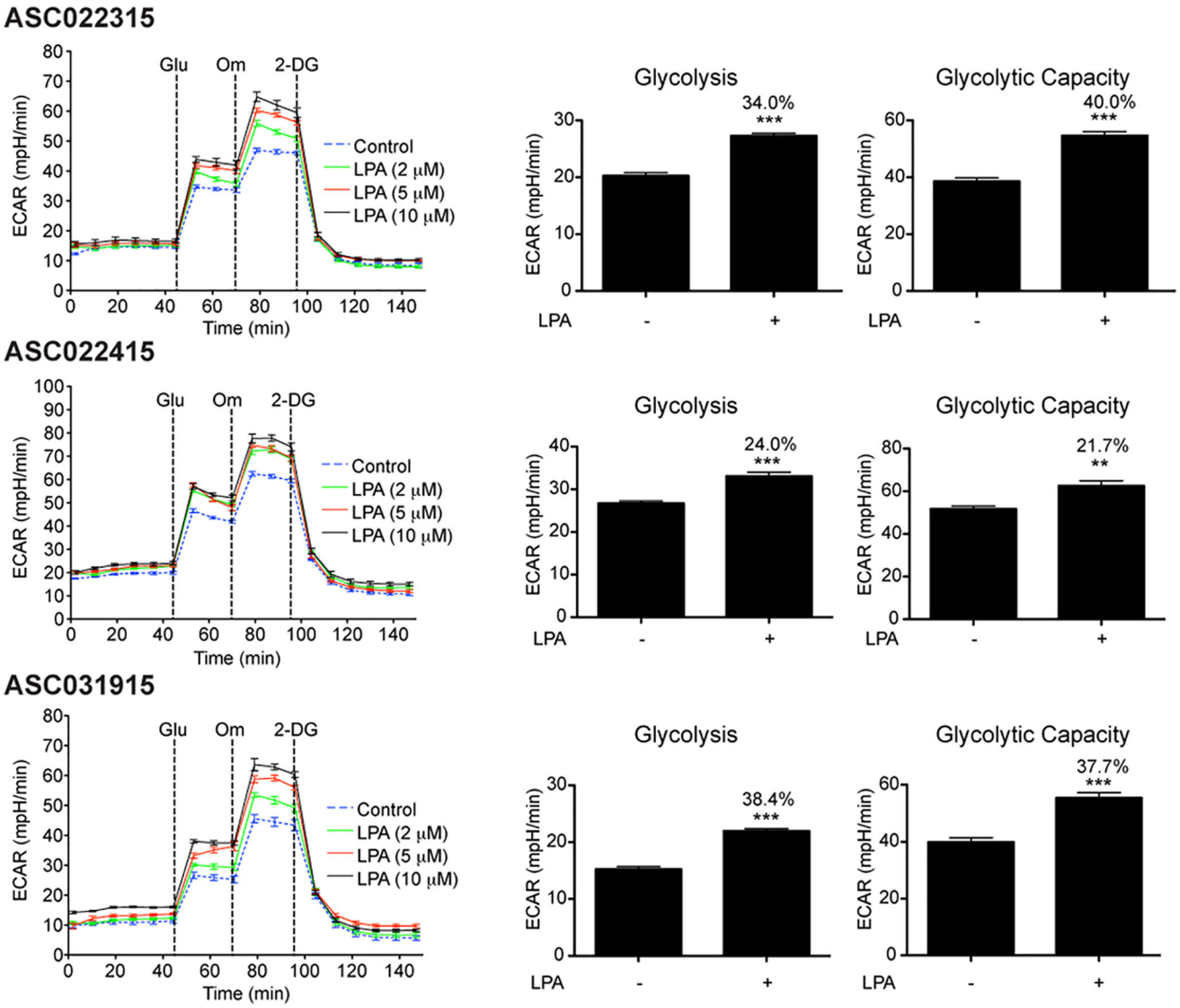

Figure 2. LPA induces aerobic glycolysis in patient-derived ovarian cancer cells

Patient-derived ovarian cancer cells, ASC022315, AS022415, and ASC031915, were serum starved overnight and stimulated with 2, 5, and 10 μM LPA for 6 h. ECAR was determined every 8 minutes. The experiment was repeated thrice and the ECAR flux (Left Panel), glycolytic rate, and glycolytic capacity (Right Panel) from a typical experiment are presented. Error bars represent SEM of the mean values (n = 5 to 8 parallel determinations). Percentile increases over the basal levels of glycolysis and glycolytic capacity are denoted over the bars of the chart. Statistical significance was determined by Student's t test (**P<0.005; ***P<0.0005).

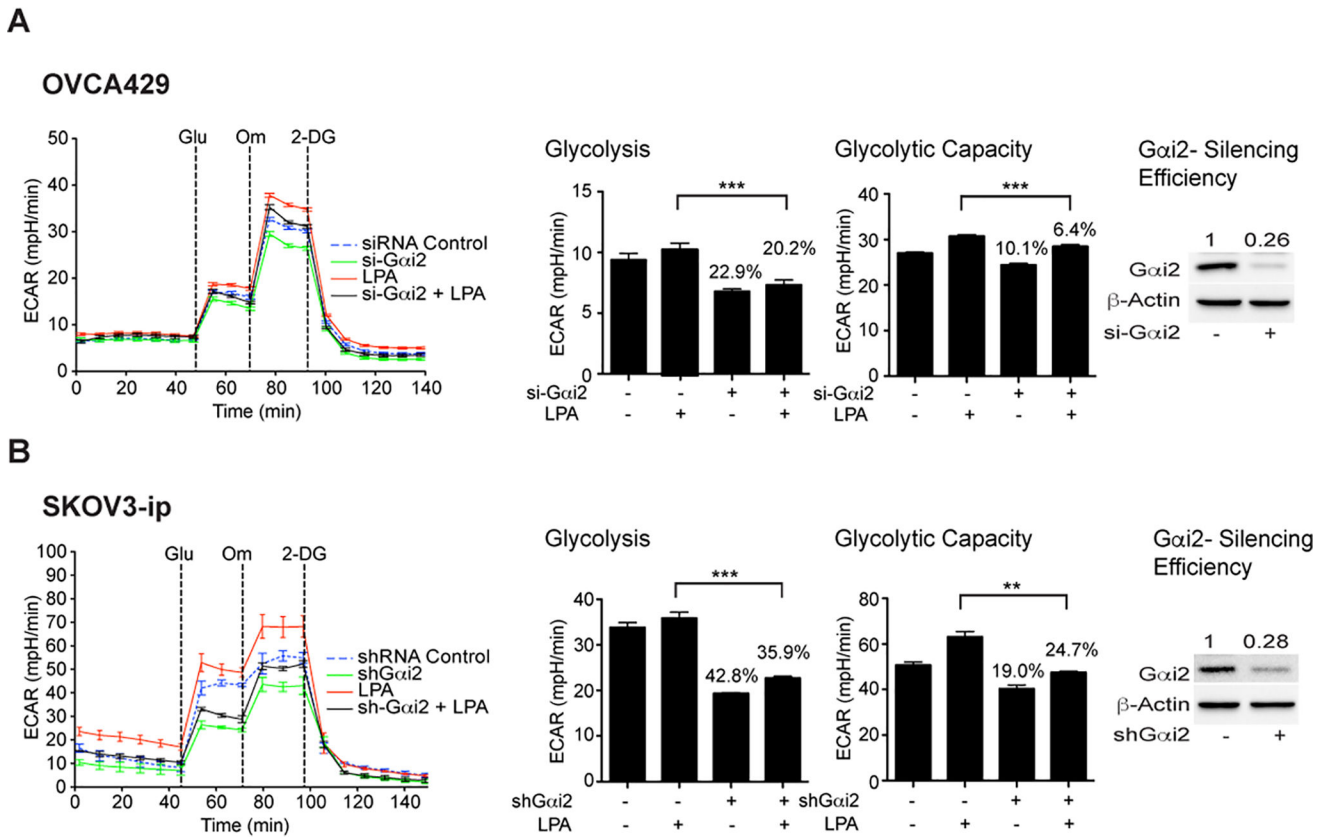

Figure 3. LPA-stimulated metabolic reprogramming involves Gαi2

A. OVCA429 ovarian cancer cells were transfected with either siRNAs targeting Gαi2 or control non-targeting siRNAs using Amaxa Nucleofector transfection method. Cells were stimulated with LPA and ECAR flux analysis was carried out as described above. ECAR flux, glycolytic rate and glycolytic capacity were plotted. The experiment was repeated at least thrice and the results are from a representative analysis (mean ± SEM, n = 10 to 11 parallel assessments). Statistical significance was determined by Student's t test (***P<0.0005). Percentile decreases over the basal levels of glycolysis and glycolytic capacity are marked above the bars of the chart. **B.** SKOV3-ip cells in which the expression of $G\alpha_{i2}$ is stably silenced with specific shRNA were serum starved overnight along with vector control cells. Cells were stimulated with LPA (10 μM) for 6 h and ECAR was determined. Results are from a typical experiment (n = 3) indicating ECAR, glycolytic rate and capacity (Mean ± SEM; n = 7 to 10 parallel determinations). Percentile decreases over the basal levels of glycolysis and glycolytic capacity are denoted above the bars of the chart. Statistical significance was determined by Student's t test (**P<0.005; ***P<0.0005). Silencing efficiency was monitored by immunoblot analysis using Gαi2-antibodies and subsequent quantification of the immunoreactive bands. Quantified values demonstrating the efficiency of silencing are presented above Gαi2 bands.

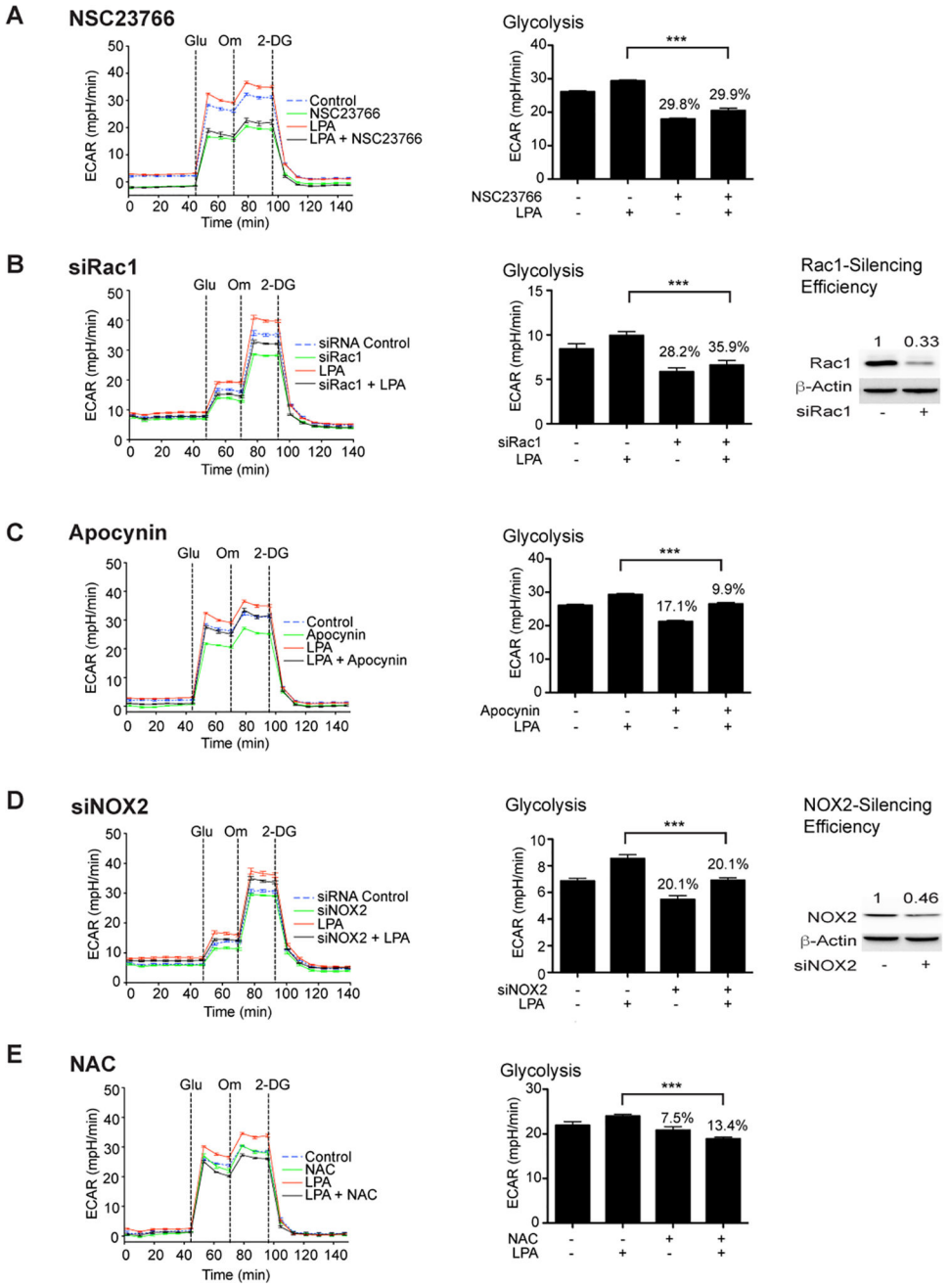

Figure 4. Regulation of glycolysis by LPA requires the Rac1-NOX-ROS network

SNU119 cells were pretreated with 10 μM Rac1-inhibitor, NSC23766 (Panel A), 100 μM NOX-inhibitor, Apocynin (Panel C), or 10 μM ROS-scavenger, N-acetyl cysteine (Panel E) for 1 hr, following which they were stimulated with LPA (10 μM) for 6 h. ECAR flux and glycolytic rate were plotted. Representative analysis from a set of three independent experiments (mean ± SEM; n = 9 parallel determinations) is presented. Statistical significance was determined by Student's t test (***P<0.0005). Percentile decreases over the basal levels of glycolytic rate are denoted above the bars of the histogram. For siRNA studies, OVCA429 cells were transfected with either siRNAs targeting Rac1 (Panel B),

NOX2 (Panel D), or control non-targeting siRNAs for 48 hrs following which they were stimulated with 10 μM LPA for 6 h. ECAR flux over time and glycolytic rate were plotted. Results (mean ± SEM; n = 9 – 11 parallel determinations) from a representative analysis (n = 3 independent experiments) are presented along with statistical significance, determined by Student's t test (***P<0.0005). Percentile decreases over the basal levels of glycolysis are marked above the bars of the histogram. Silencing efficiency was monitored by immunoblot analysis using antibodies to Rac1 or NOX2. Immunoreactive bands were quantified and the quantified expression values for Rac 1 (Panel B) and NOX2 (Panel D) are presented above the respective bands.

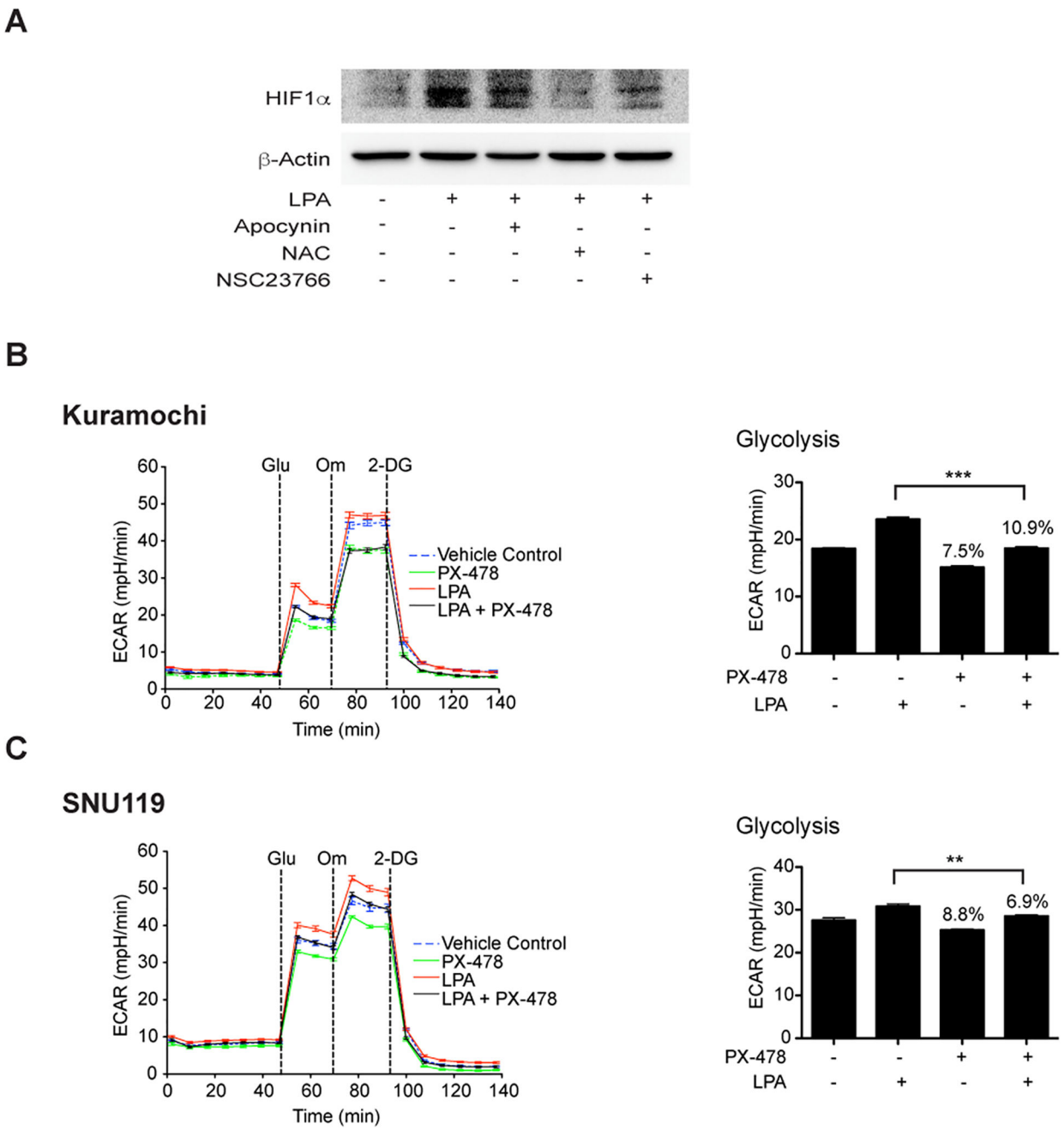

Figure 5. LPA induces pseudohypoxic increase in HIF1α via Rac1-NOX-ROS to promote aerobic glycolysis

LPA stimulates an increase in HIF1α levels through Rac1, NOX, and ROS (Panel A). SNU119 cells, pretreated with Rac-inhibitor (NSC23766, 10 μM), NOX-inhibitor (Apocynin, 100 μM), or ROS-scavenger (N-acetyl cysteine, 10 μM) for 1 hr, were stimulated with LPA (10 μM) for 6hrs along with untreated controls. Cells were lysed and immunoblot analyses were carried out with the antibodies to HIF1α. The blot was stripped and re-probed for GAPDH to ensure equal protein loading. Results from a typical experiment (n = 3) are presented in Panel A. Role of HIF1α in LPA-stimulated aerobic glycolysis was monitored using Kuramochi (Panel B) and SNU119 (Panel C) cell lines. Cells, pretreated with HIF-1α-

specific inhibitor PX-478 for 18 hours, were stimulated with LPA (10 μM) for 6 hours and ECAR analysis was carried out. ECAR flux and the rate of glycolysis were plotted (mean ± SEM; n = 9 to 12 measurements). Statistical significance was determined using Student's t test (**P<0.005; ***P<0.0005). Percentile decreases over the basal levels of glycolysis are denoted above the bars of the chart.

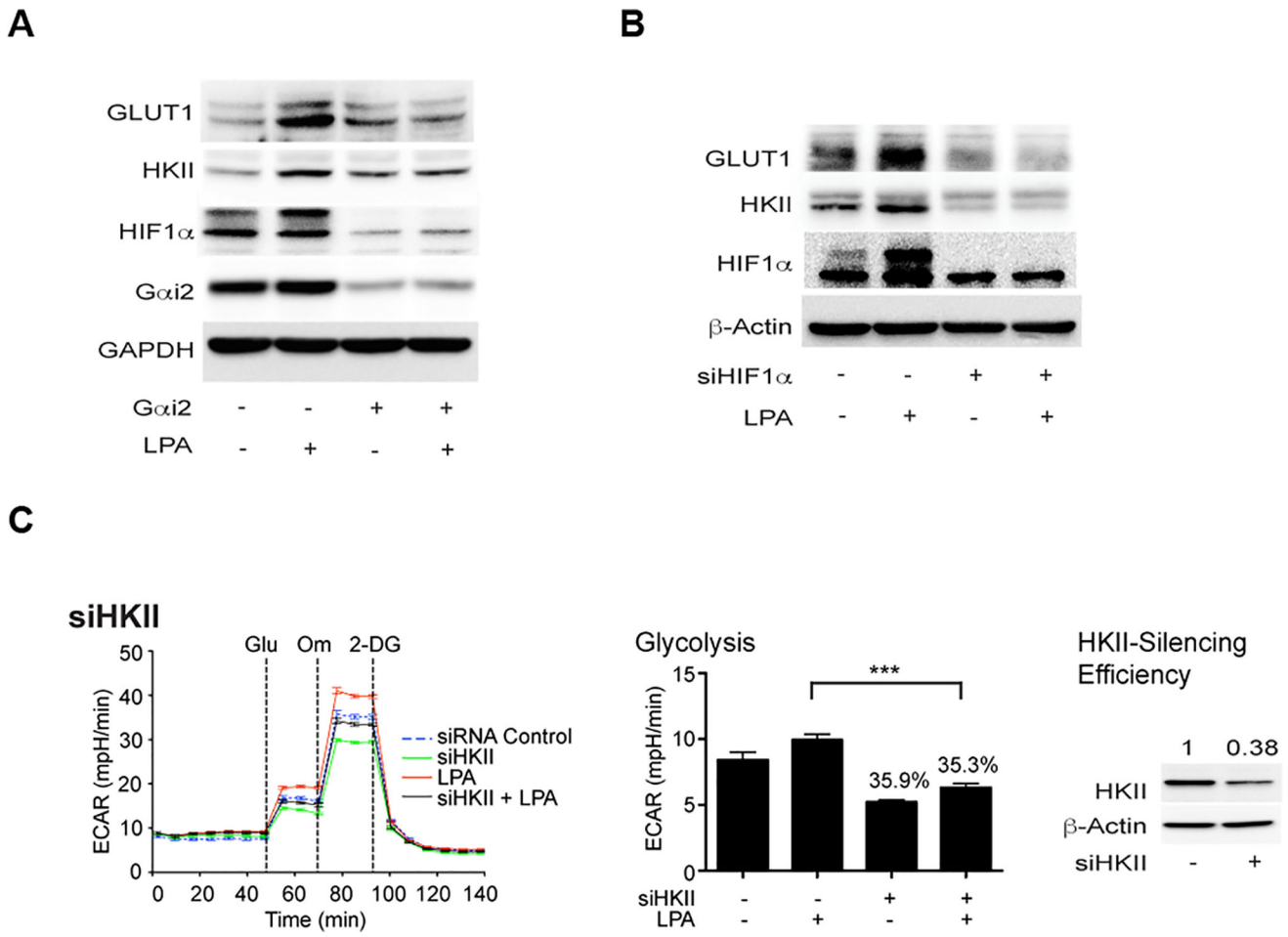

Figure 6. LPA-stimulated glycolysis involves $G\alpha_{i2}$, HIF1α, and HKII

SKOV3-ip cells were transiently transfected with control siRNA or siRNA targeting specifically si$G\alpha_{i2}$ (Panel A) or siHIF1α (Panel B) for 48 hrs. These cells were stimulated with LPA (10 μM) for 6 hrs and the lysates from these cells were subjected to immunoblot analysis using the respective antibodies. The blot was stripped and re-probed for GAPDH to monitor equal protein loading. Presented results are from a typical experiment (n = 3). To demonstrate the role of HKII in LPA-stimulated glycolysis, OVCA429 cells were transfected with siRNAs targeting HKII (Panel C) or control non-targeting siRNAs for 48 hrs following which they were stimulated with 10 μM LPA for 6 h. ECAR flux and the rate of glycolysis were plotted. Results are from a representative analysis (n = 3) and each bar represents mean ± SEM from 9 – 12 parallel determinations. Statistical significance was determined by Student's t test (***P<0.0005). Percentile decreases over the basal levels of glycolysis are denoted above the bars of the histogram. Lysates from the transfectants were processed for immunoblot analysis with HKII-antibodies to monitor the silencing efficiency of the siRNAs. Immunoreactive HKII-bands were quantified and the quantified values for the expression of HKII are marked above the HKII bands.

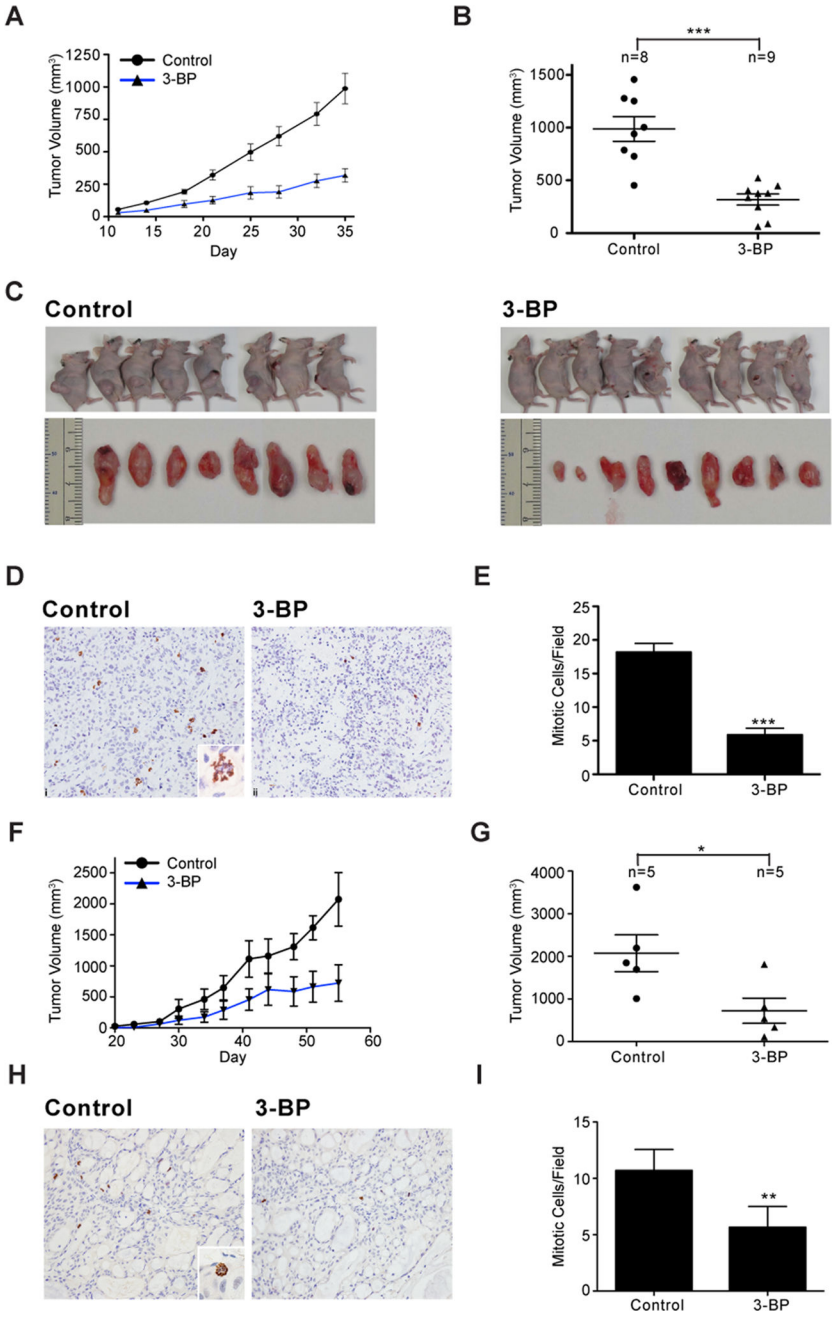

Figure 7. Inhibition of HKII using 3-BP reduces tumor progression

Nu/Nu nude female mice were injected with SKOV3-ip or OVCAR8 cells subcutaneously (5×10^6 cells) to generate tumors. At day 11 (SKOV3-ip) or 23 (OVCAR8), when the tumors reached 50 mm^3, the mice were randomized into 2 groups (SKOV3-ip; n=10, OVCAR8; n=5) and intraperitoneally administered with vehicle or 3-BP (i.p.; 10 mg/kg body weight) in two cycles. The studies were terminated before the animal welfare was compromised. Tumor growths in SKOV3-ip xenograft animals were monitored until day 35 (Panel A). Animals were sacrificed on day 35 and the tumor volumes of the animals were measured and recorded (Panel B and C). Tumors harvested from these animals were processed for

immunohistochemical analysis using anti-phosphohistone H3 antibodies (anti-PHH3) to determine the mitotic index of the cells (Panel D). Magnification of the micrograph is 20× whereas the inset is 60×. Number of mitotic cells in 5 random fields in the micrographs from each of the tumor samples were quantified using ImageJ software and the mean ± SEM values are presented (Panel E). Similar analysis was carried out with OVCAR8-xenograft tumor bearing animals. Tumor growth was monitored until day 55 (Panel F). The animals were sacrificed on day 55 before their welfare was compromised and the tumor volumes were determined (Panel G). Tumor tissue harvested from these animals were processed for PHH3-staining to determine mitotic index (Panel H). Magnification of the micrograph is 20× whereas the inset is 60×. Number of cells in the mitotic phase were quantified using ImageJ software in 5 fields of each animal tumor sample and the mean ± SEM is presented (Panel I).